

Orbital and magnetic ordering in single-layer FePS₃: A DFT+*U* study

Mohammad Amirabbasi* and Peter Kratzer†

Fakultät für Physik and CENIDE, Universität Duisburg-Essen, Lotharstraße 1, 47057 Duisburg, Germany

(Dated: December 21, 2022)

Among the numerous 2D system that can be prepared via exfoliation, iron phosphorus trisulfide (FePS₃) attracts a lot of attention recently due to its broad-range photoresponse, its unusual Ising-type magnetic order and possible applications in spintronic nano-devices. Despite various experimental and theoretical-computational reports, there are still uncertainties in identifying its magnetic ground state. In this paper, we investigate the structural and magnetic properties of single-layer FePS₃ by using Density Functional Theory. Our findings show that orbital ordering leads to a variation in distance between pairs of iron atoms by 0.14 Å. These lattice distortions, albeit small, trigger different (ferromagnetic and antiferromagnetic) exchange couplings so that the ground state consists of ferromagnetically aligned zigzag chains along the long Fe – Fe bonds which couple antiferromagnetically along the shorter Fe – Fe bonds. Within the DFT+*U* framework, we parameterize a spin Hamiltonian including Heisenberg, single-ion anisotropy, Dzyaloshinskii-Moriya and biquadratic interactions. Using $U = 2.22$ eV gives a consistent description of both the electronic band gap and the Neel temperature in 2D FePS₃.

I. INTRODUCTION

The study of two-dimensional (2D) magnetic ground states has gained special interest after the discovery of stable long-range ferromagnetic (FM) and antiferromagnetic (AFM) order in monolayer CrI₃ and FePS₃, respectively^{1,2}. The ideal candidates for 2D magnets are layered van der Waals materials such as the transition-metal dichalcogenides³, chromium trihalides¹ and transition-metal phosphorous trichalcogenides⁴. These materials hold significant promise for technological applications, especially in the field of spintronics and nanomagnetism⁵. Therefore, a deep understanding of the magnetic exchange mechanisms in 2D system is essential. In this way, it is possible to find out which exchange coupling controls the magnetic properties of the ground state and how the system selects a special order when decreasing the temperature. Here, we investigate the magnetic ordering in FePS₃, a 2D Ising antiferromagnet with a Neel temperature of 116 – 120 K in bulk^{6,7}. In advantage over other 2D materials, Ramos *et al.*⁸ claimed the optical response of FePS₃ over a broad range of the electromagnetic spectrum, from infrared to ultraviolet: Its band gap of about 1 eV^{8–11} makes FePS₃ suitable for infra-red detection while applications in ultraviolet photodetectors¹² and in non-linear optics¹³ have been reported as well. In addition, pure bulk FePS₃ displays antiferromagnetic ordering below 120 K^{6,14} while its magnetic and structural properties can be tuned easily¹⁵ by chemical modification. That's why this material, similar to the low-temperature 2D magnet CrI₃, is a suitable candidate for the next step in spintronics towards AFM 2D spintronic devices⁵ operating at low temperatures.

From the structural point of view, bulk FePS₃ is a 2D layered material. Fig. 1 shows the unit cell of one monolayer. To visualize the crystal structure, it is better to write Fe₂P₂S₆, which means that in each layer, every Fe ion is surrounded by bipyramidal (P₂S₆)^{4–} anions. In

this way, each Fe is octahedrally bonded to six S atoms while each P is bonded to three S atoms and one P atom.

The Fe²⁺ ions in FePS₃ have the maximum magnetic moment compatible with their charge state, i.e. their spin is $S = 2$. Leaving away all the other ions for clarity, the positions of the Fe²⁺ ions, and thus of their spins, can be described by a distorted honeycomb lattice. Two opposite sides of each hexagon are slightly (between 0.017 Å and 0.19 Å according to different experimental sources^{14,17}) longer than the other four sides, see Fig. 2. This difference has a crucial effect on the type of magnetic exchange interaction between Fe atoms. Another important feature of the magnetism in FePS₃ is its strong out-of-plane easy axis, which renders stable magnetic order even in the monolayer limit. According to the Hohenberg-Mermin-Wagner theorem^{18,19} in a system with isotropic interactions, thermal fluctuations in 2D would prevent the spontaneous symmetry breaking required to form a low-temperature ordered state. Therefore, some anisotropic interaction, e.g. magnetic single-ion anisotropy, is required in 2D systems to get a ground state with long-range magnetic order¹. However, despite many experimental and theoretical investigations^{14,20–26}, the magnetic unit cell of the ground state of FePS₃ is still under debate. Leaving aside possible complications in the three-dimensional material related to stacking order, several authors^{14,22} assumed an identity of the structural and the magnetic unit cell, containing two Fe²⁺ ions each. Consequently, all Fe – Fe bonds along a ferromagnetically aligned chain would be identical in length. In contrast, LeFlem *et al.*²³ proposed a unit cell with four Fe²⁺ ions in which the ferromagnetically aligned Fe chains run along an alternating sequence of short and long Fe – Fe bonds. This proposal was taken up later by other researchers^{27–29}, e.g. to explain the observation of Brillouin-zone folding effects in measured Raman spectra⁷. Note that the FM chains in both models are rotated by 60° in the plane, see Fig. 3.

The so far unresolved issue of the relation between

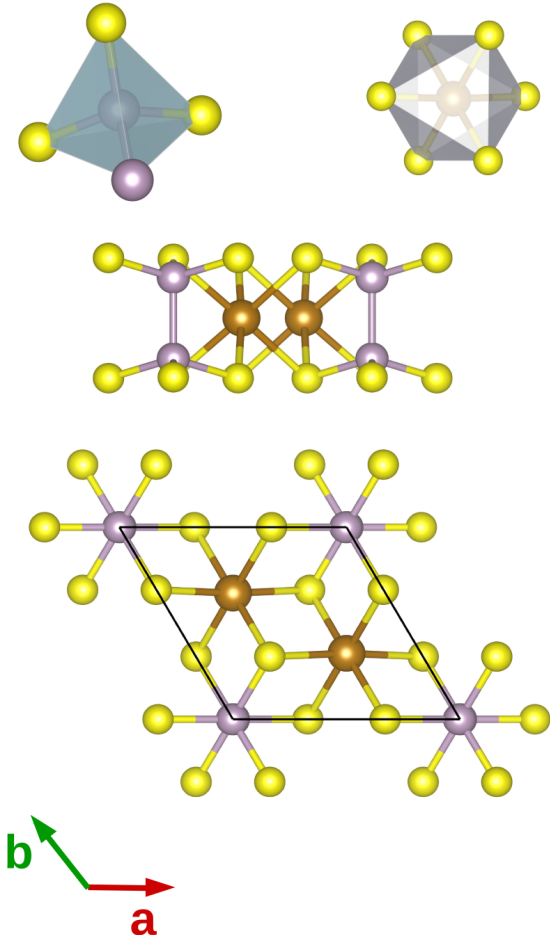


FIG. 1: (Color online) (**Top row**) Octahedral and tetrahedral environment of Fe and P ions in FePS_3 , respectively. The primitive cell of the FePS_3 monolayer (**Middle**) in side view and (**Bottom**) in top view. The brown, grey and yellow spheres denote the Fe, P and S atoms, respectively. Each Fe atom is surrounded by six S ions. The P dimer, oriented perpendicular to the plane of view, sits in the center of the Fe honeycomb. Magnetic exchange interactions between Fe ions are governed by the S ions as the mediating links between them. Data in this figure, as well as in figures 3, 4 and 7, were drawn using the VESTA software¹⁶.

lattice distortion and magnetic ground state motivated us to carry out a comprehensive computational study of the magnetic properties employing the DFT+ U approach (Density Functional Theory plus on-site electron-electron repulsion). In the literature, spin model Hamiltonians had considered exchange interactions only up to the third-nearest neighbors of the Fe atoms^{20,21}, and the difference between short and long Fe – Fe bonds had been ignored in the Hamiltonian parameterization. Moreover, higher-order (in the spin variable) couplings, such as the Dzyaloshinskii-Moriya interaction and bi-quadratic couplings, had been neglected so far. We find that $U = 2.22$ eV can produce the experimental band gap of 1.23 eV. Interestingly, we find that the magnetic exchange interaction is ferromagnetic and antiferromag-

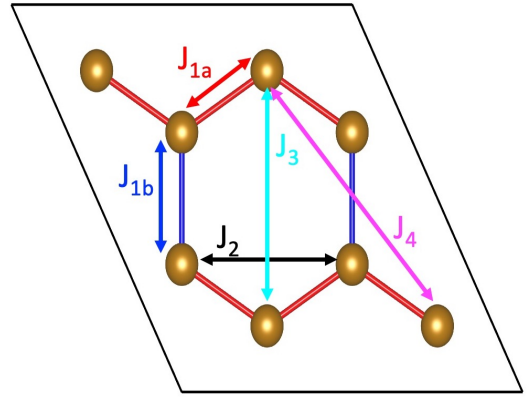


FIG. 2: (Color online) Simplified representation of the FePS_3 crystal structure showing only the Fe atoms. A (2×2) cell is depicted, allowing us to show the (slightly) distorted honeycomb geometry in which Fe ions sit at each vertex. The red and blue color marks short and long bonds, respectively, differing by about 4% in length. The magnetic exchange constants J_i are indicated by the double arrows.

netic along the long bonds and short bonds, respectively. This assignment turns out to be robust with respect to changes in the U parameter. We conclude that the magnetic ground state consists of ferromagnetic spin chains running along the long bonds that couple antiferromagnetically among each other. In addition, we propose a model spin Hamiltonian that includes anisotropic spin interactions that are of crucial importance of 2D magnets, as well as an interaction up to fourth neighbors, such that the fall-off of magnetic interactions with distance, as it is expected for a magnetic insulator, can be seen.

The paper is structured as follows. In section II the details of the DFT and Monte Carlo calculations are presented. Section III is devoted to electronic properties as well as the derivation of the spin Hamiltonian and the different aspects of exchange interactions in the determination of the magnetic ground state of the FePS_3 monolayer. Finally, In section IV a summary is given.

II. COMPUTATIONAL DETAILS

As a single crystal, iron phosphorous trichalcogenide crystallizes in the monoclinic structure with space group $C2/m$. The Fe atoms occupy the $4g(0,y,0)$ sites, P atoms occupy the $4i(x,0,z)$ and S atoms occupy $4i(x,0,z)$ and $8j(x,y,z)$ sites, respectively. Structural parameters can be found in Ref. 14. We used the so-defined lattice parameters and atomic positions as starting point for our calculations of a FePS_3 monolayer. To generate an isolated layer, the lattice parameter perpendicular to the layers (c -axis) of the bulk structure was increased to 20 Å.

We employ two different computational approaches for our first-principles calculations: For calculating the single-site magnetic anisotropy and anisotropic interac-

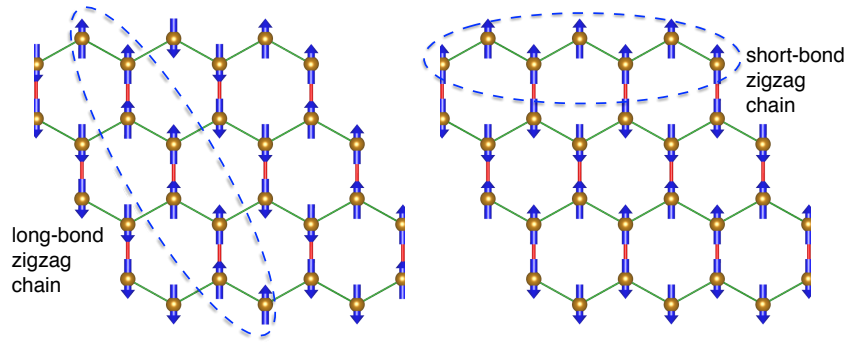


FIG. 3: (Color online) The sublattice of Fe atoms in FePS₃ forms a distorted honeycomb structure. The blue arrows indicate the orientation of the Fe magnetic moments. The Fe – Fe bonds marked by red (thicker) lines are about 4% longer than those marked by green (thinner) lines. The **(left)** long-bond zigzag chain and **(right)** short-bond zigzag chain encircled by the blue, dashed ellipses propagate along the crystallographic *b*-axis or *a*-axis, respectively.

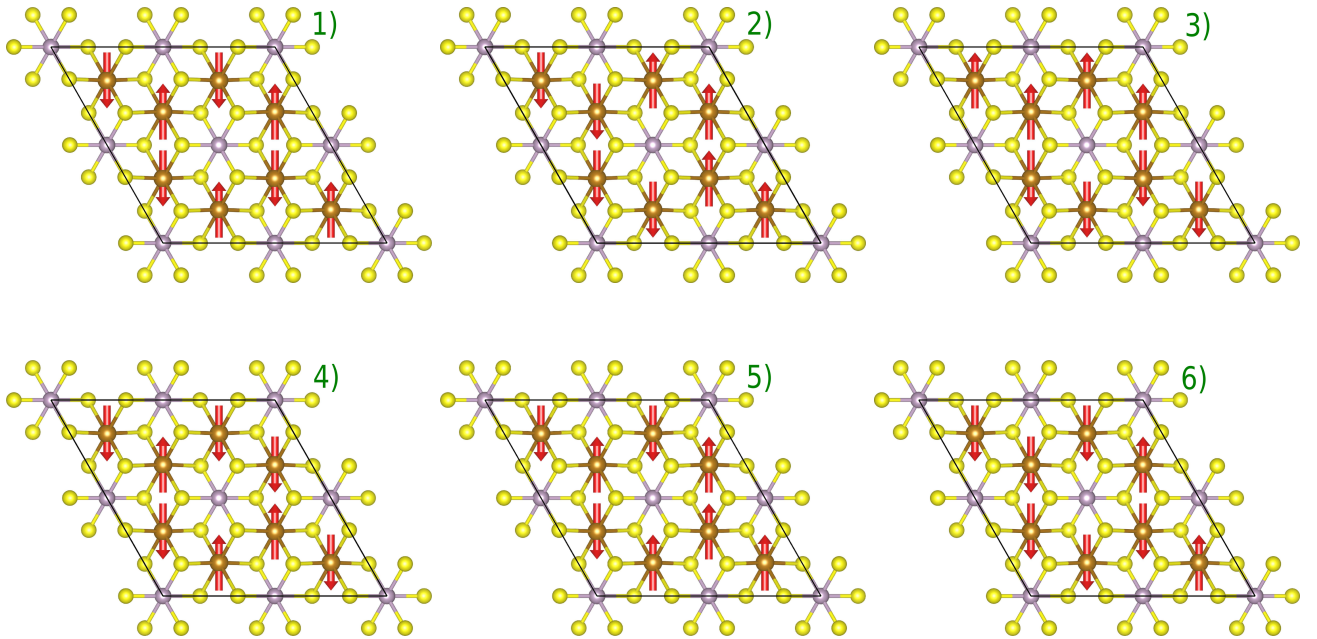


FIG. 4: (Color online) Different collinear magnetic configurations that we use for obtaining J parameters. The yellow, grey and brown spheres are S, P and Fe ions, respectively. The red arrow shows the direction of the magnetic moment on each Fe ion. Note that some Fe–Fe distances (the vertical ones in the plots) are about 4% larger than the others, and hence all six configurations shown are non-equivalent. **Top row** shows (from left to right) Neel, long-bond zigzag and short-bond zigzag configurations. Our DFT+ U calculations show that the long-bond zigzag is the global minimum ground state. **Bottom row** shows additional collinear configurations considered.

tions between spins that rely on a relativistic description of electrons as well as for the biquadratic interaction which needs a non-collinear scheme, we use an all-electron full-potential linearized augmented plane-wave (FP-LMTO) method. For large systems consisting of many atoms with collinear spins, computationally more efficient calculations were carried out with the Quantum-Espresso (QE)³² code in the framework of the spin-polarized density functional theory. We approximate the exchange-correlation energy using the generalized gradient approximation (GGA) in the Perdew-Burke-

Ernzerhof parameterization³³. For a better description of the low-temperatures ground state of FePS₃, we used GGA+ U approach to correct on-site electron-electron interaction (U) for the $3d$ orbitals of the Fe atoms, following Dudarev’s approach which includes a spherically symmetric effective on-site Coulomb repulsion U_{eff} . Since QE is a plane-wave code, GBRV ultra-soft pseudopotentials³⁴ for the elements Fe, P, and S are employed to describe the interaction of the valence electrons with the ionic core. The optimized cut-off energies of 50 Ry and 480 Ry have been used for expanding the wavefunctions

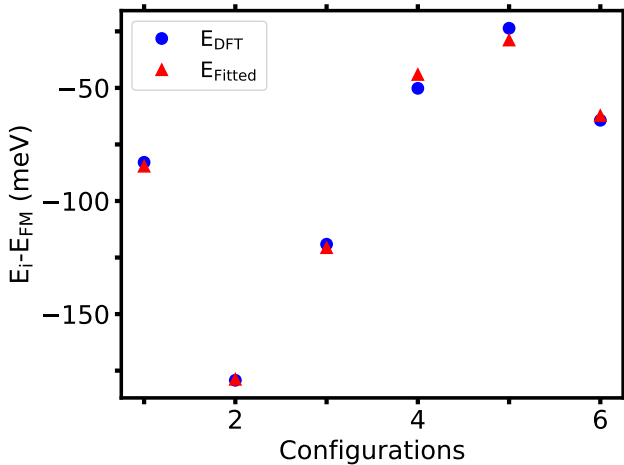


FIG. 5: (Color online) This figure illustrates how total energies of different collinear configurations obtained by means of DFT+ U calculations are mapped to a Heisenberg Hamiltonian^{30,31}. With this mapping, we can calculate the J parameters for various neighbor shells. The numbered spin configurations correspond to those shown in Fig. 4. The energies plotted in the graph are for $U_{\text{eff}}=2.22$ eV. The standard fitting error for each U_{eff} is ~ 2

%.

TABLE I: Optimized nearest-neighbor distances obtained from DFT+ U calculations using $U = 2.22$ eV of the long-bond zigzag ground state compared to distances determined experimentally from Ref. 14. For the derivation of the spin Hamiltonian, the different lengths of nearest-neighbor bonds d_{1a} and d_{1b} are considered by different exchange interactions J_{1a} and J_{1b} while the same exchange constant is used for all atoms in the second to fourth neighbor shell.

	this work	experimental ¹⁴
d_{1a} (Å)	3.44	3.36
d_{1b} (Å)	3.58	3.55
d_2 (Å)	6.02, 6.05	5.93, 5.94
d_3 (Å)	6.92, 7.00	6.71, 6.92
d_4 (Å)	9.17, 9.18, 9.33	8.96, 9.04, 9.17

and charge density, respectively, in plane waves.

Some magnetic modelling parameters, such as the single-ion anisotropy (SIA) and the Dzyaloshinskii-Moriya (DMI), require the inclusion of spin-orbit interaction, and therefore a relativistic treatment of the electrons. For an accurate treatment of these aspects, we employ the full-potential linearized augmented plane wave (FP-LMTO) method, as implemented in the FLEUR code³⁵. The cut-off energy of the plane-wave expansion in the interstitial region is set to $k_{\text{max}} = 3.8$ a.u.⁻¹. The muffin-tin radii of Fe, P and S atoms are set to 2.8, 1.49 and 1.90 a.u., respectively. Although the FLEUR code allows for a more general treatment of the on-site electron-electron interaction, we chose to set the on-site Hund exchange to zero to stay compatible with the QE

calculations.

In order to determine the type of magnetic order of the ground state, we define a model spin Hamiltonian :

$$H_{\text{spin}} = H_{\text{Heis}} + \frac{1}{2}B \sum_{\text{n.n}} (\vec{S}_i \cdot \vec{S}_j)^2 + \frac{1}{2}D \sum_{\text{n.n}} \hat{D}_{ij} \cdot (\vec{S}_i \times \vec{S}_j) + \Delta \sum_i (\vec{S}_i \cdot \vec{d}_i)^2 \quad (1)$$

where \vec{S}_i represents direction of magnetic spins, H_{Heis} is the usual Heisenberg Hamiltonian (for details see below), B , D and Δ are the strengths of biquadratic, DMI and SIA, respectively. Moreover, unit vectors \hat{D}_{ij} and \vec{d}_i show the direction of the DMI and the easy axis of magnetization at each site i , respectively. It should be noted that the direction of DMI is determined by Moriya rules³⁶. Due to the centrosymmetric 2/m point group symmetry, the FePS₃ monolayer has a mirror plane perpendicular to the b -axis. According to the Moriya rules, when a mirror plane includes two ions, the D vector should be perpendicular to the mirror plane.

For the determination of B , D and Δ with FLEUR, we consider the primitive cell (2 Fe atoms, 10 atoms in total) and a $10 \times 10 \times 1$ Monkhorst-Pack k-point mesh. The biquadratic interaction originates from electron hopping, and in terms of a tight-binding description it can be obtained in fourth order from a perturbation theory^{37,38}. For extracting the B term from DFT calculations, we rotate the spins of the two Fe atoms pointing in opposite direction around the c -axis in such a way that the sum of them remains zero, $S_1 + S_2 = 0$. In this way, the energy due to the Heisenberg term is degenerate and the total energy differences are attributed to B only. It should be noted that in the calculation of B spin-orbit coupling (SOC) has not been considered, and the anisotropic terms are quenched. For the anisotropic exchange interactions, we need to consider the effect of SOC (GGA+ U +SOC). Care must be taken in the selection of appropriate spin configurations that allow us to extract the values of D and Δ from total energy differences. Therefore, pairs of configurations are constructed in such a way that their energies, as given by the Heisenberg term, are degenerate before turning on SOC. For SIA, we consider a pair of magnetic configurations in which all spins are oriented along the c -axis or along the b -axis, respectively. For these configurations, the DMI term vanishes in GGA+ U +SOC calculations. For obtaining the strength of D , we need to consider two different magnetic configurations in which two spins are oriented on the a -axis and the negative b -axis for the first, and the a -axis and the positive b -axis for the second one. In this way, the Δ term vanishes in GGA+ U +SOC calculations. From energy difference of each pair of configurations, the Δ and D can be extracted.

With the aim to characterize the low-temperature magnetic ground state of FePS₃, Monte Carlo simulations of classical spins on a lattice have been performed using

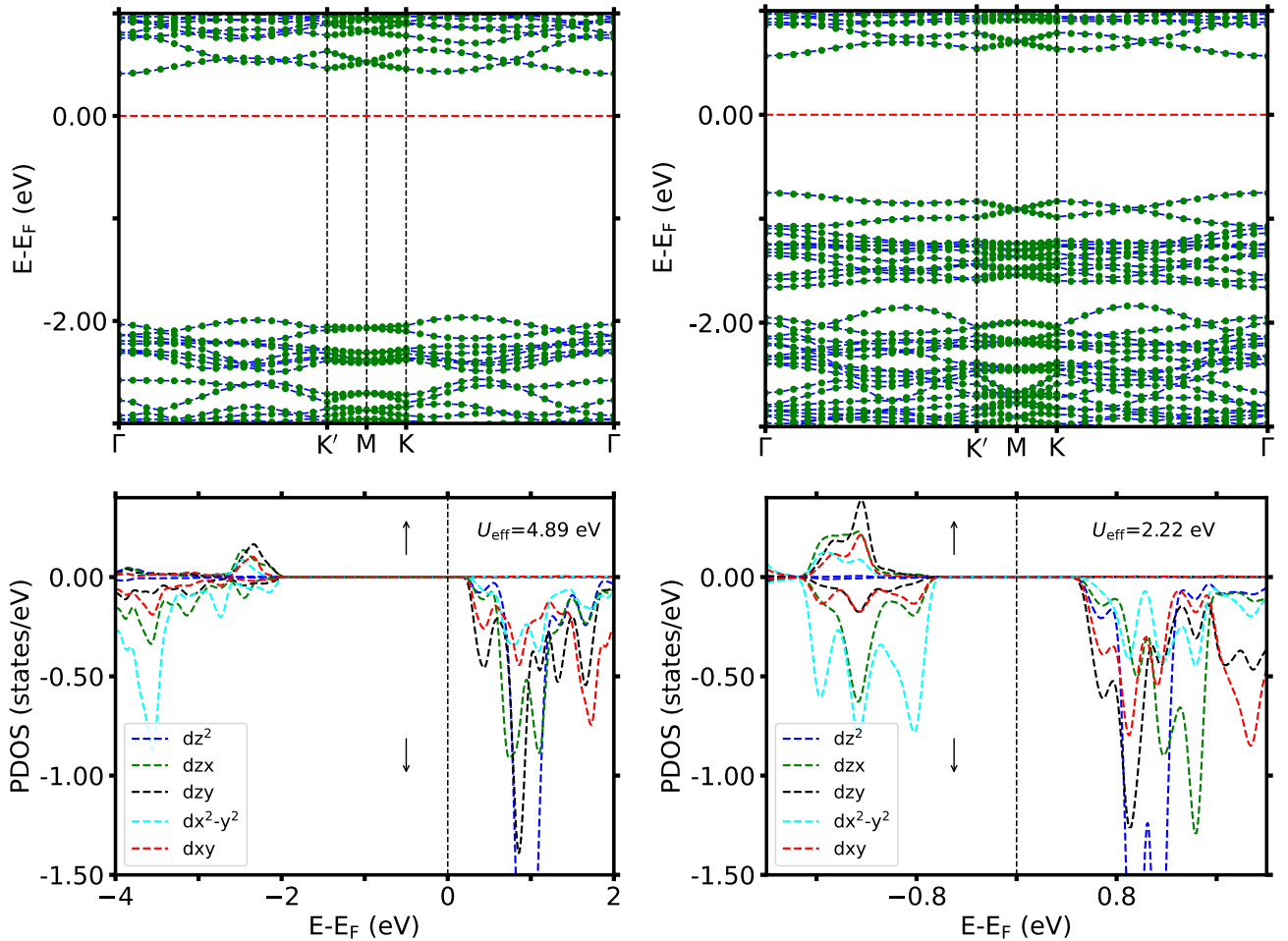


FIG. 6: (Color online) **Top row** Bandstructure and (**Bottom row**) projected density of states (PDOS) of the AFM long-bond zigzag structure for $U_{\text{eff}} = 4.89$ and 2.22 eV, respectively. For bandstructures, the green and blue colors denote spin up and spin down, respectively. Due to the absolute spin being zero for AFM long-bond zigzag, the two spin channels collapse to each other. When U_{eff} is decreased, the contribution of the $d_{x^2-y^2}$ orbital to the highest occupied bands increases. This is the reason why in the bandstructure with $U_{\text{eff}} = 2.22$ eV the two topmost valence bands are split off. These calculations were done in the (2×2) cell also used for the calculations of the J parameters.

the replica-exchange method³⁹. We use two-dimensional lattices consisting of $N \times L^2$ spins, where $L = 10$ is the linear size of the simulation cell and N is the number of spins ($N = 2$ for the primitive cell). For checking phase transition at low temperature, different sizes of the simulation cell from $L = 8$ to $L = 14$ are considered. For the thermal equilibrium and data collection, we consider 3×10^6 Monte Carlo steps (MCs) per spin at each temperature.

III. RESULTS AND DISCUSSION

A. Geometric and electronic structure

It is well known from previous studies that in FePS_3 the Fe^{2+} ions are in the high-spin state of Fe. Conse-

quently at one Fe atom five electrons are pointing spin-up while one electron is spin-down and occupies a single $3d$ orbital. Of course, at Fe atoms with opposite magnetic moment the role of spin-up and spin-down electrons is interchanged. Due to the rather large distance between the Fe^{2+} ions, the interaction between the $3d$ orbitals of different Fe ions is weak, yet decisive for the magnetic ground state. Since the energies of the orbitals on the $3d$ shell are split up by the crystal field of the surrounding sulfur anions, unequal occupation of the $3d$ orbitals, and hence orbital ordering, are to be expected. Thus, the DFT+ U method is mandatory for a correct description of electronic structure. Several approaches are possible to determine a suitable value for U : We found that we are able to reproduce the experimental band gap by choosing $U = 2.22$ eV. For this purpose, we rely on the most recent experimental value of 1.23 eV⁸, discarding

an older optical absorption measurement that had estimated a band gap of ~ 1.6 eV¹⁰ as outdated. This value of U is of the same order as the value $U = 2$ eV used in Ref. 20. Alternatively, we estimated U using Density Functional Perturbation Theory (DFPT)⁴⁰ which is implemented in the QE code. This calculation has been done by considering the primitive cell of FePS₃ (containing 10 atoms), and a value of $U = 4.89$ eV is obtained. Since the DFT+ U calculations have been done using two codes, we compared the obtained gap to make sure that different implementations of DFT+ U have no effect on the results. The gaps obtained from the QE and FLEUR code are in good agreement for each U parameter.

We started by performing a number of explorative calculations to investigate the interplay between structure and magnetic order at low temperature. For this purpose we used a (1×2) cell which includes four Fe ions and allows us to build ferromagnetic zigzag chains of spins, either running along the long or the short Fe – Fe separations, as illustrated in Fig. 3. We started from the experimental geometry¹⁴ and optimized the geometry using self-consistent forces obtained with the GGA+ U method. In particular, we optimized both the lattice vectors and the positions of the atoms in the cell for both spin configurations shown in Fig. 3. In both cases, it is found that the Fe – Fe distances are unequal; two opposing edges of the Fe hexagons are longer than the others by 0.14 Å and 0.13 Å for 'long-bond' and 'short-bond' spin configurations, respectively. The lattice constants determined for the two spin structures differ by less than 0.4%. Having spins ferromagnetically aligned in the zigzag chain passing through the long Fe-Fe bonds is found to be always energetically more favorable than the alignment along the short bonds, or any other spin structure in this cell. Moreover, we find this trend to be independent on the value of U . To construct the spin Hamiltonian, it is therefore justified to work with the optimized lattice constants and atomic positions of the ground-state spin configuration, the long-bond zigzag chain, and to use this fixed geometry for all others. The optimized distances between the Fe atoms which are used to derive J parameters are summarized in Table I. Using $U = 2.22$ eV, the two different nearest neighbor distances are determined as $d_{1a} = 3.44$ Å and $d_{1b} = 3.58$ Å, see Fig. 2. Thus, the obtained results show that the distance between the nearest Fe neighbors differs by $d_{1b} - d_{1a} = 0.14$ Å; this agrees well with the structure determination by neutron scattering at low temperature by Lançon *et al.*¹⁴ who obtained 0.19 Å while earlier experiments¹⁷ using X-ray diffraction at room temperature in magnetically disordered samples had found a smaller value of 0.017 Å. We will later argue that this distortion has a crucial effect on exchange interaction and magnetic properties of the ground state. The obtained lattice parameters for the primitive unit cell ($a = 6.017$ Å and $b = 6.052$ Å and $\gamma = 119.86^\circ$) are in good agreement with experimental values¹⁴ of bulk samples ($a = 5.940$ Å and $b = 5.972$ Å and $\gamma = 121.29^\circ$).

Calculations of the electronic band structure and the

orbital-projected density of states of the magnetic ground state for both values of U are shown in Fig. 6. While the band structure obtained with $U = 2.22$ eV reproduces the experimental gap of 1.23 eV, the calculation with $U = 4.89$ eV gives a much wider band gap. The projected density of states show that for $U = 2.22$ eV this gap is opened up by the intra-atomic Coulomb repulsion between the occupied $3d_{x^2-y^2}$ orbitals and the remaining unoccupied $3d$ orbitals. For the larger U_{eff} value, the occupied $3d$ state of Fe is pushed down even further in energy and energetically overlaps with the valence bands, hence the larger band gap encountered in this case. A Löwdin analysis indicates that all $3d$ states for spin majority are fully occupied while for spin minority the Löwdin charges in the individual orbitals for $U_{\text{eff}} = 4.89$ eV are 0.03, 0.35, 0.18, 0.60, 0.15 for d_{z^2} , d_{xz} , d_{yz} , $d_{x^2-y^2}$ and d_{xy} , respectively. By decreasing the U_{eff} parameter, the hybridization between the $3d$ orbitals of Fe and the p orbitals of P and S slightly weaker, so that for $U_{\text{eff}} = 2.22$ eV the $d_{x^2-y^2}$ orbital has less mixing with other orbitals, and the respective Löwdin charges are 0.02, 0.31, 0.13, 0.61, and 0.15. We conclude that $U_{\text{eff}} = 2.22$ eV is a suitable choice to concurrently reproduce both the crystal structure and the electronic structure of the AFM FePS₃ monolayer.

As indicated by the Löwdin charges in the $U_{\text{eff}} = 2.22$ eV case, only a single orbital of the $3d$ shell, the in-plane $d_{x^2-y^2}$ orbital, is occupied. Thus, the electronic ground state of FePS₃ shows orbital ordering. To illustrate its role, a partial charge density plot of the highest occupied band at the Γ point is displayed in Fig. 7. It shows that the spatial orientation of the in-plane Fe $3d$ orbital with respect to the crystal axes changes between the two Fe atoms in the structural unit cell. In addition, sulfur p orbitals oriented within the plane are involved in forming this electronic band. The alternating rotation of the Fe $3d$ orbital allows for a bonding overlap (same sign of the orbital lobes) between the S atom and both Fe atoms for the long Fe – Fe distance in the distorted hexagon. This finding explains why the long-bond zigzag chain is energetically preferred. Another aspect of orbital ordering is the unusually large orbital moment of Fe in this system. Using the Berry curvature approach⁴¹, we find the orbital moment of each Fe to equal 0.77 and 0.8 μ_B for $U_{\text{eff}} = 2.22$ eV and 4.89 eV, respectively. We believe that the reason for such a large orbital moment can be understood in analogy to the orbital moment of a free Fe atom which is determined by Hund's rule. In this system, Fe²⁺ is in a $3d^6$ state. We thus expect 4 μ_B as spin moment, and DFT yields 3.46 μ_B for $U_{\text{eff}} = 2.22$ eV. The difference is related to induced magnetic moments at the S and P ions. Moreover, for $3d^6$ the quantum numbers m_l do not add up to zero, which means the orbital moment is not quenched and points perpendicular to the plane. As a consequence, the effect of SOC and its related exchange interactions cannot be neglected, and there is a strong tendency for the spin to align with the orbital moment perpendicular to the plane.

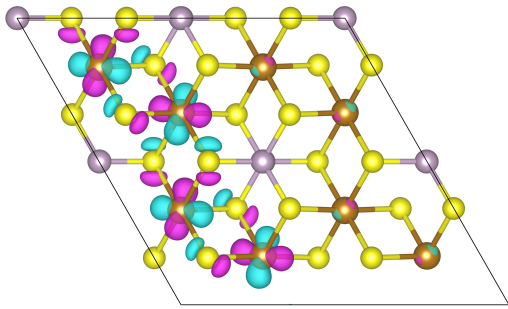


FIG. 7: (Color online) Iso-contour plot of the wavefunction (shown only in the left part of the cell for clarity) of the highest valence band at the Γ point. The overlap between the $d_{x^2-y^2}$ orbital of Fe ions and the p orbitals of the S ions changes its sign. This is the reason why AFM and FM interactions alternate along the chain.

Because of the sensitivity to orbital ordering, we found out that great care must be taken when converging the electronic self-consistency cycle in the DFT+ U calculation. In particular, the choice of the starting point for the density matrix used to represent the electronic state of the single spin-down electron in the DFT+ U scheme has an influence on the converged result and must be checked carefully.

B. Magnetic exchange interactions

Next we map the information obtained from our DFT+ U calculations onto a Heisenberg Hamiltonian

$$H_{\text{spin}} = -\frac{1}{2} \sum_{i \neq j} J_{ij} (\vec{S}_i \cdot \vec{S}_j) \quad (2)$$

Motivated by the orbital ordering leading to 'long' and 'short' distances between Fe neighbors, we allow for a differentiation of the first-neighbor J parameters into J_{1a} (= 'short') and J_{1b} (= 'long') interactions. Since previous calculations had indicated a rather long range of the exchange interactions, despite the semiconducting character of FePS₃, we decided to include interactions up to the fourth-nearest neighbors. Therefore, collinear magnetic configurations were calculated in a quite large (2×2) supercell using the QE code. The total energies for all possible 15 collinear structures were calculated to find the global minimum. The six configurations lowest in energy shown in Fig. 4 were used to determine five exchange parameters. Note that, unlike in previous work^{20,21} the so-called 'stripy' magnetic pattern was not included in the fit because our calculations indicate that its energy is much higher than those of the other configurations.

C. Spin Hamiltonian and Monte Carlo simulation

Now we proceed to discuss the features of the effective spin Hamiltonian, to find the ground state in a large simulation cell, and to calculate the finite-temperature properties of FePS₃ monolayer. To avoid any ambiguity due to the debatable value of the U parameter, we investigate the dependence of the properties on this parameter systematically, varying it between the value determined from the band gap, $U = 2.22$ eV, and the value from DFPT, $U = 4.89$ eV. Table II summarizes calculated H terms for the different U_{eff} parameters, as well as T_N and Curie-Weiss temperature (θ_{CW}), which has been obtained by means of MC simulations using the Hamiltonian of Eq. 1.

For all U_{eff} parameters, exchange interaction for J_{1a} and J_{1b} is AFM and FM, respectively. This means that FM chains run along the long Fe – Fe bond and couple to each other antiferromagnetically along the short bond. This is in agreement with the long-bond zigzag ground state²³. Interestingly, some interactions are antiferromagnetic (J_{1a} and J_3 , negative sign), while others are ferromagnetic (J_{1b} and J_4 , positive sign). The value of J_4 is the smallest, thus ensuring that the magnetic exchange interaction falls off with distance, as one would expect in an insulating material. In absolute terms, J_3 has the largest value, larger than J_{1a} . The dominance of J_3 , which is responsible for the preferred antiparallel spin alignment between neighboring chains is getting even more prominent when a small value of U (as dictated by the experimentally known electronic band gap) is employed. Remarkably, the small difference between d_{1a} and d_{1b} goes along with a different sign of the interactions J_{1a} and J_{1b} , the latter being ferromagnetic. While this may seem surprising at first, we note that also in other 2D magnetic systems, such as Cr-trihalides, it has been reported that the exchange parameter may change its sign if the bond distances and bond angle change even by small amounts⁴⁴. In a wider context, this can be seen as a consequence of the Kanamori-Anderson-Goodenough rules⁴⁵⁻⁴⁷ that emphasize the role of the bond angle at the anion connecting two cations. The governing principle is the dependence of the exchange interaction on the orientation of the anion p orbital relative to the bond axis between the magnetic cations. For more long-ranged interactions, the connectivity of the lattice sites (mediated via the $3p$ orbitals of P and S ions) governs the super-exchange mechanism. According to the strong-coupling perturbation theory, adding an extra intermediate ion (site-connection) increases the order of the perturbative expansion. Therefore, the super-exchange interaction does not reach zero with increasing distances as quickly as in other materials, e.g. in oxides.

As can be seen from Tab. II, the strengths of Δ and D increase with decreasing U_{eff} which satisfies Anderson's rule⁴⁶. Previous reports^{14,20,25} didn't mention the effect of DMI in this system. They considered only the effect of the out-of-plane SIA which is responsible for the sym-

TABLE II: Calculated Heisenberg couplings J_i (meV) up to the fourth neighbors, biquadratic exchange interaction B (meV), Dzyaloshinskii-Moriya exchange interaction D (meV) and single ion anisotropy Δ (meV) for different U_{eff} (eV) parameters. Negative and positive value denotes anti-ferromagnetic and ferromagnetic exchange interaction, respectively. Note that $|S| = 1$ has been used in the definition of the spin Hamiltonian. Using the obtained couplings, we perform MC simulations to find the Curie-Weiss (θ_{CW}) and Neel (T_N) temperatures (K). We compare to experimental data from Ref. ^{6,7,42,43}.

U_{eff}	J_{1a}	J_{1b}	J_2	J_3	J_4	Δ	D	B	T_N	θ_{CW}
4.89	-3.48	3.63	-0.67	-3.62	0.29	0.71	-0.57	-1.00	48.88	-67.25
3.89	-3.87	3.98	-1.14	-4.01	0.20	0.73	-0.39	-1.37	51.42	-73.12
2.89	-3.80	4.13	-1.30	-5.11	0.66	0.80	-0.36	-1.80	63.80	-85.01
2.22	-3.26	4.01	-1.24	-5.71	1.50	0.89	-0.34	-2.10	70.00	-101.57
exp.									104 - 120	-112

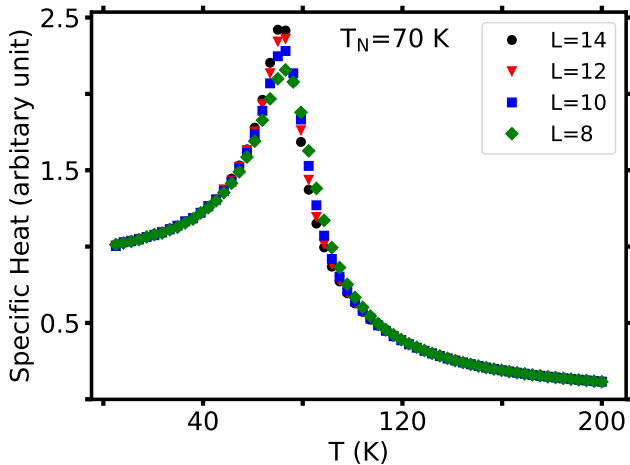


FIG. 8: (Color online) Plot of the specific heat versus temperature obtained from Monte Carlo simulations of the spin Hamiltonian for lattices with the linear sizes $L = 8$ to $L = 14$ for $U_{\text{eff}}=2.22$ eV. The divergence, seen as a peak of specific heat in the simulations, is used to read off the Neel temperature. The observation that the peak height increases with increasing L is indicative of a phase transition.

metry breaking required to have an ordered ground state in a 2D system. Here, our calculations show that the direction of the D vector is along the c -axis due to the lack of inversion symmetry and helps SIA to break rotational symmetry. Our MC simulations show that without considering the effect of Δ and D , at finite temperature not all spins are oriented perpendicular to the plane. Besides increasing T_N , the effect of Δ and D is to create perfect Ising-AFM order with spins pointing along the c -axis. The negative value of B favours the collinear coupling of spins. This feature also helps the system to settle in the Ising-AFM state. The presence of a biquadratic interaction in FePS₃ has been suggested by Wildes *et al.*²⁷ when analyzing the experimental neutron scattering pattern and magnetoelastic effect.

As a major result of the Monte Carlo simulations, we present the temperature dependence of the specific heat in Fig. 8 for $U_{\text{eff}}=2.22$ eV. The value of T_N is estimated

from the location of the peak. We observe that this peak becomes higher by increasing the simulation lattice size which is a confirmation of a phase transition taking place. We obtain the Curie-Weiss temperatures (θ_{CW}) by a linear fitting of the inverse susceptibility in the temperature range between 150 K to 300 K. The negative values of θ_{CW} indicate that the ground state has AFM order. In addition, θ_{CW} increases monotonically with decreasing U_{eff} which can be related to the enhancement of exchange interactions, in good agreement with Anderson's theory of super-exchange⁴⁶. According to the definition⁴⁸ of the frustration index $f = \frac{|\theta_{\text{CW}}|}{T_N}$, it is between 1 to 10 for all U_{eff} , indicating that this is a lightly frustrated system.

While the obtained θ_{CW} is close to the experimental value, the obtained T_N for $U_{\text{eff}}=2.22$ eV still falls short of the experimentally measured value. We note that other reports of first-principles based MC simulations for this material have also not been fully successful to obtain the exact Neel temperature²⁰. A possible reason could be the neglect of spin-phonon coupling⁴⁹⁻⁵¹ in our simulation. If FePS₃ undergoes a spin-Peierls transition, a gap in the magnetic excitation spectrum would result that is indeed observed in inelastic neutron scattering experiments¹⁴. Taking the gapped excitation spectrum into account, we expect a higher Neel temperature. However, simulations incorporating the quantum nature of joint phononic and magnetic excitations are beyond the scope of our current work.

IV. CONCLUSION

In summary, using DFT calculations we determined a spin Hamiltonian for a single layer of FePS₃ with Heisenberg exchange up to the fourth neighbor, the nearest-neighbor DM and biquadratic interactions and single-ion anisotropy. The three latter terms jointly result in the preferred alignment of Fe magnetic moments perpendicular to the crystallographic plane which has led to the characterization of FePS₃ as an Ising antiferromagnet. A series of calculations with different values U_{eff} of the on-site Coulomb interactions in the Fe $3d$ shell has been carried out to ensure the robustness of the results. All

calculations show that due to orbital ordering the honeycomb lattice formed by the Fe atoms is not ideal; two opposite sides of the Fe hexagons are longer than the others. We observe that calculated magnetic exchange couplings along the long bonds and short bonds are AFM and FM, respectively. As a consequence, the magnetic ground state must be described by a unit cell with (at least) four Fe atoms and consists of chains of parallel magnetic moments running across the long bonds. In an attempt to reproduce both the electronic band gap and the Neel temperature, we conclude that a value of $U_{\text{eff}} = 2.22\text{eV}$ is a reasonable choice, but there is room for improvement by including more subtle effects such as spin-lattice coupling.

V. ACKNOWLEDGMENT

We gratefully acknowledge the computing time granted by the Center for Computational Sciences and Simulation

(CCSS) of the University of Duisburg-Essen and provided on the supercomputer magnetUDE (DFG Grant No. INST 20876/209-1 FUGG and INST 20876/243-1 FUGG) at the Zentrum für Informations- und Mediendienste (ZIM). M. A. was supported by a fellowship from Universität Duisburg-Essen and thanks his colleagues who provided insight and expertise that greatly assisted the research. The guidelines provided by Dr. Hyun-Jung Kim and Dr. Gustav Bhilmayer are gratefully acknowledged by M. A.

-
- * Electronic address: mo.amirabbasi@gmail.com
 † Electronic address: Peter.Kratzer@uni-due.de
- ¹ B. Huang, G. Clark, E. Navarro-Moratalla, D. R. Klein, R. Cheng, K. L. Seyler, D. Zhong, E. Schmidgall, M. A. McGuire, D. H. Cobden, W. Yao, D. Xiao, P. Jarillo-Herrero, and X. Xu, *Nature* **546**, 270 (2017).
 - ² C. Gong, L. Li, Z. Li, H. Ji, A. Stern, Y. Xia, T. Cao, W. Bao, C. Wang, Y. Wang, Z. Q. Qiu, R. J. Cava, S. G. Louie, J. Xia, and X. Zhang, *Nature* **546**, 265 (2017).
 - ³ M. Chhowalla, H. S. Shin, G. Eda, L.-J. Li, K. P. Loh, and H. Zhang, *Nature Chemistry* **5**, 263 (2013).
 - ⁴ W.-B. Zhang, Q. Qu, P. Zhu, and C.-H. Lam, *J. Mater. Chem. C* **3**, 12457 (2015).
 - ⁵ E. C. Ahn, *npj 2D Materials and Applications* **4**, 17 (2020).
 - ⁶ J.-U. Lee, S. Lee, J. H. Ryoo, S. Kang, T. Y. Kim, P. Kim, C.-H. Park, J.-G. Park, and H. Cheong, *Nano Letters* **16**, 7433 (2016).
 - ⁷ X. Wang, K. Du, Y. Y. F. Liu, P. Hu, J. Zhang, Q. Zhang, M. H. S. Owen, X. Lu, C. K. Gan, P. Sengupta, C. Kloc, and Q. Xiong, *2D Materials* **3**, 031009 (2016).
 - ⁸ M. Ramos, F. Carrascoso, R. Frisenda, P. Gant, S. Mañas-Valero, D. L. Esteras, J. J. Baldoví, E. Coronado, A. Castellanos-Gomez, and M. R. Calvo, *npj 2D Materials and Applications* **5**, 19 (2021).
 - ⁹ C. R. S. Haines, M. J. Coak, A. R. Wildes, G. I. Lampronti, C. Liu, P. Nahai-Williamson, H. Hamidov, D. Daisenberger, and S. S. Saxena, *Phys. Rev. Lett.* **121**, 266801 (2018).
 - ¹⁰ R. Brec, D. M. Schleich, G. Ouvrard, A. Louisy, and J. Rouxel, *Inorganic Chemistry* **18**, 1814 (1979).
 - ¹¹ P. Foot, J. Suradi, and P. Lee, *Materials Research Bulletin* **15**, 189 (1980).
 - ¹² Y. Gao, S. Lei, T. Kang, L. Fei, C.-L. Mak, J. Yuan, M. Zhang, S. Li, Q. Bao, Z. Zeng, Z. Wang, H. Gu, and K. Zhang, *Nanotechnology* **29**, 244001 (2018).
 - ¹³ D. Xu, Z. Guo, Y. Tu, X. Li, Y. Chen, Z. Chen, B. Tian, S. Chen, Y. Shi, Y. Li, C. Su, and D. Fan, *Nanophotonics* **9**, 4555 (2020).
 - ¹⁴ D. Lançon, H. C. Walker, E. Ressouche, B. Ouladdiaf, K. C. Rule, G. J. McIntyre, T. J. Hicks, H. M. Rønnow, and A. R. Wildes, *Phys. Rev. B* **94**, 214407 (2016).
 - ¹⁵ M. Cheng, Y.-S. Lee, A. K. Iyer, D. G. Chica, E. K. Qian, M. A. Shehzad, R. dos Reis, M. G. Kanatzidis, and V. P. Dravid, *Inorganic Chemistry* **60**, 17268 (2021).
 - ¹⁶ K. Momma and F. Izumi, *Journal of Applied Crystallography* **44**, 1272 (2011).
 - ¹⁷ W. Klिंगen, G. Eulenberger, and H. Hahn, *Zeitschrift für anorganische und allgemeine Chemie* **401**, 97 (1973).
 - ¹⁸ N. D. Mermin and H. Wagner, *Phys. Rev. Lett.* **17**, 1307 (1966).
 - ¹⁹ P. C. Hohenberg, *Phys. Rev.* **158**, 383 (1967).
 - ²⁰ T. Olsen, *Journal of Physics D: Applied Physics* **54**, 314001 (2021).
 - ²¹ B. L. Chittari, Y. Park, D. Lee, M. Han, A. H. MacDonald, E. Hwang, and J. Jung, *Phys. Rev. B* **94**, 184428 (2016).
 - ²² K. Kurosawa, S. Saito, and Y. Yamaguchi, *Journal of the Physical Society of Japan* **52**, 3919 (1983).
 - ²³ G. Le Flem, R. Brec, G. Ouvrard, A. Louisy, and P. Segransan, *Journal of Physics and Chemistry of Solids* **43**, 455 (1982).
 - ²⁴ J. min Zhang, Y. zhuang Nie, X. guang Wang, Q. lin Xia, and G. hua Guo, *Journal of Magnetism and Magnetic Materials* **525**, 167687 (2021).
 - ²⁵ A. R. Wildes, K. C. Rule, R. I. Bewley, M. Enderle, and T. J. Hicks, *Journal of Physics: Condensed Matter* **24**, 416004 (2012).
 - ²⁶ K. C. Rule, G. J. McIntyre, S. J. Kennedy, and T. J. Hicks, *Phys. Rev. B* **76**, 134402 (2007).
 - ²⁷ A. R. Wildes, M. E. Zhitomirsky, T. Ziman, D. Lançon, and H. C. Walker, *Journal of Applied Physics* **127**, 223903 (2020).
 - ²⁸ C. Murayama, M. Okabe, D. Urushihara, T. Asaka, K. Fukuda, M. Isobe, K. Yamamoto, and Y. Matsushita, *Journal of Applied Physics* **120**, 142114 (2016).

- ²⁹ G. Ouvrard, R. Brec, and J. Rouxel, *Materials Research Bulletin* **20**, 1181 (1985).
- ³⁰ X. Li, H. Yu, F. Lou, J. Feng, M.-H. Whangbo, and H. Xiang, *Molecules* **26** (2021), 10.3390/molecules26040803.
- ³¹ A. Sadeghi, M. Alaei, F. Shahbazi, and M. J. P. Gingras, *Phys. Rev. B* **91**, 140407 (2015).
- ³² P. Giannozzi, S. Baroni, N. Bonini, M. Calandra, R. Car, C. Cavazzoni, D. Ceresoli, G. L. Chiarotti, M. Cococcioni, I. Dabo, A. D. Corso, S. de Gironcoli, S. Fabris, G. Fratesi, R. Gebauer, U. Gerstmann, C. Gougoussis, A. Kokalj, M. Lazzeri, L. Martin-Samos, N. Marzari, F. Mauri, R. Mazzarello, S. Paolini, A. Pasquarello, L. Paulatto, C. Sbraccia, S. Scandolo, G. Sclauzero, A. P. Seitsonen, A. Smogunov, P. Umari, and R. M. Wentzcovitch, *Journal of Physics: Condensed Matter* **21**, 395502 (2009).
- ³³ J. P. Perdew, K. Burke, and M. Ernzerhof, *Phys. Rev. Lett.* **77**, 3865 (1996).
- ³⁴ K. F. Garrity, J. W. Bennett, K. M. Rabe, and D. Vanderbilt, *Computational Materials Science* **81**, 446 (2014).
- ³⁵ FLEURgroup, "<http://www.flapw.de/>," .
- ³⁶ T. Moriya, *Phys. Rev.* **120**, 91 (1960).
- ³⁷ F. Mila and F.-C. Zhang, *The European Physical Journal B - Condensed Matter and Complex Systems* **16**, 7 (2000).
- ³⁸ K. Tanaka, Y. Yokoyama, and C. Hotta, *Journal of the Physical Society of Japan* **87**, 023702 (2018).
- ³⁹ K. Hukushima and K. Nemoto, *Journal of the Physical Society of Japan* **65**, 1604 (1996).
- ⁴⁰ I. Timrov, N. Marzari, and M. Cococcioni, *Phys. Rev. B* **98**, 085127 (2018).
- ⁴¹ A. Malashevich, I. Souza, S. Coh, and D. Vanderbilt, *New Journal of Physics* **12**, 053032 (2010).
- ⁴² P. Jernberg, S. Bjarman, and R. Wappling, *Journal of Magnetism and Magnetic Materials* **46**, 178 (1984).
- ⁴³ P. A. Joy and S. Vasudevan, *Phys. Rev. B* **46**, 5425 (1992).
- ⁴⁴ B. Sadhukhan, A. Bergman, Y. O. Kvashnin, J. Hellsvik, and A. Delin, *Phys. Rev. B* **105**, 104418 (2022).
- ⁴⁵ J. Kanamori, *Journal of Physics and Chemistry of Solids* **10**, 87 (1959).
- ⁴⁶ P. W. Anderson, *Phys. Rev.* **79**, 350 (1950).
- ⁴⁷ J. B. Goodenough, *Phys. Rev.* **100**, 564 (1955).
- ⁴⁸ A. P. Ramirez, *Annual Review of Materials Science* **24**, 453 (1994).
- ⁴⁹ L. Webster, L. Liang, and J.-A. Yan, *Physical Chemistry Chemical Physics* **20**, 23546 (2018).
- ⁵⁰ F. Ferrari, R. Valentí, and F. Becca, *Phys. Rev. B* **104**, 035126 (2021).
- ⁵¹ X. Xu, X. Wang, P. Chang, X. Chen, L. Guan, and J. Tao, *The Journal of Physical Chemistry C* **126**, 10574 (2022).